# SoC CMOS UWB Pulse Radar Sensor for Contactless Respiratory Rate Monitoring

Domenico Zito, *Member, IEEE*, Domenico Pepe, *Member, IEEE*, Martina Mincica, *Student Member, IEEE*, Fabio Zito, Alessandro Tognetti, Antonio Lanatà, and Danilo De Rossi, *Member, IEEE*

*Abstract*—An ultra wideband (UWB) system-on-chip radar sensor for respiratory rate monitoring has been realized in 90 nm CMOS technology and characterized experimentally. The radar testchip has been applied to the contactless detection of the respiration activity of adult and baby. The field operational tests demonstrate that the UWB radar sensor detects the respiratory rate of person under test (adult and baby) associated with sub-centimeter chest movements, allowing the continuous-time non-invasive monitoring of hospital patients and other people at risk of obstructive apneas such as babies in cot beds, or other respiratory diseases.

*Index Terms*—Biomedical monitoring, CMOS technology, contactless sensing, sleep apnea, ultra-wideband radar.

## I. INTRODUCTION

ONE of the world-wide research priorities for the up-coming years will be dealing with ageing, including health systems, medical technologies and rare diseases complemented by other areas like developing personalized medicines approaches aimed at improving safety and quality of life. One of the most relevant objectives associated with such research consists also of the opportunity of gaining a better understanding of ageing, tackling chronic diseases, e.g., those linked to ageing, and adapting healthcare systems to meet specific needs. The general aim is to support the development and/or proof of principle of technologies for application in the area of personalized medicine, i.e., tailored medical interventions more effective with fewer side effects. Technologies should be of use in research, screening, diagnostics and/or guidance and therapeutic interventions.

In the frame of these research priorities for Health theme [1], a significant role is expected to be played by Information and Communication Technology (ICT). In particular, microelectronics is expected to contribute with new classes of mass-market sensors and their applications in support of disease prevention and early detection, rehabilitation and healthy lifestyle, so becoming the main driver of the next-generation health-care systems. Thanks to the technology scaling, nano-scale CMOS has led to consistent improvements of device density and performance, emerging over the last years as the predominant technology of the microelectronic industry [2]. As result of this on-going trend, innovative high-performance, highly miniaturized and low-cost sensors are expected in order to deal with the challenges regarding the needs of innovative continuous-time monitoring systems and diagnostic tools in medicine. One of the key areas of needs is related with the implementation of non-invasive sensors for contactless detection of vital signs and ultra low-power wireless data communication among sensors.

Representative of such needs, in 2002 the Federal Communications Commission (FCC) gave the permission for operating and marketing of a new class of devices incorporating ultra wideband (UWB) technology [3] and allocating a 7.5 GHz-wide bandwidth in the radiofrequency range from 3.1 to 10.6 GHz. UWB devices are thought for several applications, such as ground penetrating radar, surveillance, wall and through-wall imaging, high data rate communication and medical imaging. Therefore, UWB is expected to be one of the most important technologies capable of supporting both the needs of contactless sensing and ultra low-power data communication, opening to interesting opportunities for implementing innovative sensors applied to the continuous monitoring of vital parameters and their communication within wireless body area networks.

In this frame, particularly relevant is the interest in sensors for contactless respiratory rate monitoring. Such devices are expected to be the enabling technology for a wide range of continuous bio-monitoring applications, ranging from sleep wake classifications of drivers in vehicles [4] to respiratory disorder diagnoses (e.g., obstructive apneas [5]) of infants and adults, from fatigue detection for fitness users to health monitoring of patients in hospital and domestic environment (see Fig. 1). The contribution expected from continuous-time contact-less monitoring systems free of any encumbrance will have a pivoting role in tackling respiratory chronic diseases and gaining a better

D. Zito is with the Department of Electrical and Electronic Engineering, University College Cork, Cork, Ireland and also with the Tyndall National Institute, "Lee Maltings", Dyke Parade, Cork, Ireland (e-mail: domenico.zito@tyndall.ie).

D. Pepe is with the Tyndall National Institute, "Lee Maltings", Cork, Ireland.

M. Mincica was with the Department of Information Engineering, University of Pisa, 56122 Pisa, Italy and a visiting Ph.D. student at Tyndall National Institute, "Lee Maltings", Dyke Parade, Cork, Ireland. She is now with Analog Devices, Limerick, Ireland.

F. Zito was with the Department of Information, Mathematics, Electronics and Transportation, University "Mediterranea" of Reggio Calabria, 89060 Reggio Calabria, Italy. He is now with Ansaldo STS SpA, 80147 Naples, Italy.

A. Tognetti, A. Lanatà, and D. De Rossi are with the Interdepartmental Research Center "E. Piaggio", University of Pisa, 56126 Pisa, Italy.

Color versions of one or more of the figures in this paper are available online at http://ieeexplore.ieee.org.

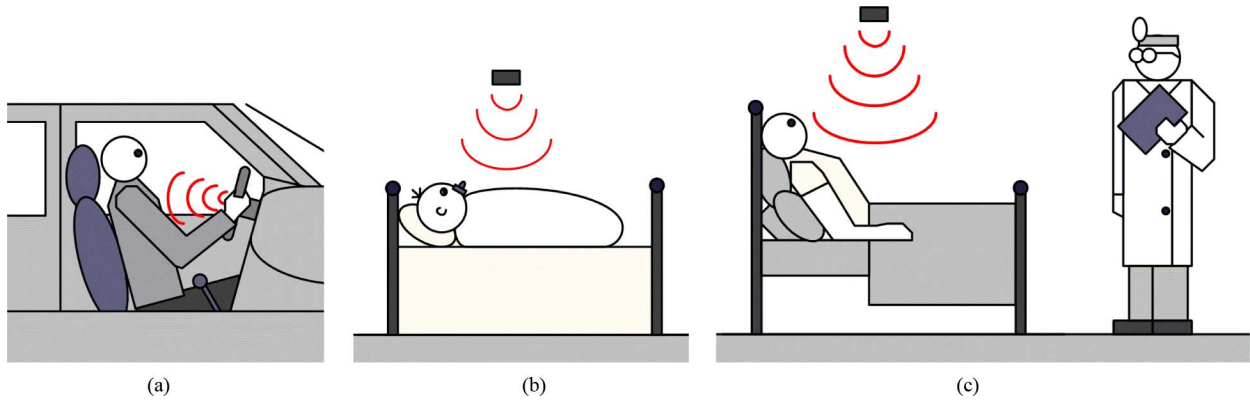Digital Object Identifier 10.1109/TBCAS.2011.2176937

Fig. 1. Examples of possible application scenarios. (a) Drivers in vehicles. (b) Babies in cot beds. (c) Patients in hospitals.

understanding of respiratory rate variability, especially in correlation with other pathological (e.g., cardiovascular, obesity, diabetes, etc.), behavioral and environmental risk factors.

This paper reports a system-on-chip (SoC) UWB pulse radar for respiratory rate monitoring implemented in 90 nm CMOS technology [6] and its experimental tests in operating scenarios. The paper is organized as follows. Section II presents the SoC UWB pulse radar system for respiratory monitoring. It reports in short the state of the art for pulse radar systems for contactless vital parameters monitoring and describes the operating principle, design and measurements of the proposed solution. The experimental results of the field operational tests on adult and baby are reported and discussed in Section III. Finally, the conclusions are drawn in Section IV.

## II. SoC UWB Pulse Radar

Pulse radars operate by sending short electromagnetic pulses and receiving the echoes reflected by the target. The time delay between transmitted pulse and received echo is given by the time of flight of the pulse (round trip from transmitter to receiver) which is therefore proportional to the distance from the target to the radar. Examples of pulse radars based on switch-gated receiver implemented by means of discrete components and applied to the detection of vital parameters are reported in literature [7], [8]. Due to the potential in terms of resolution and extremely low level of EIRP spectral density ($< -41.3$ dBm/MHz), UWB radars are very attractive for a large set of civil and military sensing applications, such as biomedical imaging, surveillance, localization, intra-wall and through-wall detections and ground penetrating. Moreover, with respect to continuous wave (CW) radars, UWB radar transceivers present a lower circuit complexity since no frequency conversions are required, leading to lower power consumption ($P_C$) for longer battery autonomy.

Thanks to implementation of efficient building blocks, in particular the pulse generator [9], our research group presented recently for the first time a UWB pulse radar front-end based on a correlation receiver, fully integrated in 90 nm CMOS technology, tested and working [6]. Hereinafter we recall some implementation details of such SoC UWB pulse radar for reasons of self-consistency and then we focus on the experimental results, reporting for the first time the evidences of field operational tests on adult (both genders) and baby volunteers.

### A. System Description

Fig. 2 shows the block diagram of the UWB pulse radar sensor, which has been implemented to be used mainly (but not only) for contactless detection of vital signs such as respiration [6]. The pulse generator (PG) transmits short pulses towards the target (i.e., human body) with a pulse repetition frequency ($f_{PR}$). The signals reflected by the target are captured by the RX antenna, amplified by the LNA and correlated (multiplied and integrated) with a delayed replica of the transmitted pulses generated on-chip by the Shaper (see Fig. 2). The signal at the output of the multiplier is integrated in order to increase the signal-to-noise ratio (SNR) and capture the envelope containing the information on the movement rate. Since vital signs vary within a few Hertz, an integrator with a 3-dB band ($B_{3dB}$) of 100 Hz allows an accurate detection. In practice, the integrator is implemented by means of a low-pass filter with bandwidth B. Averaging a large number of pulses (in the order of $f_{PR}/B_{3dB}$) allows us to increase the $SNR_{out}$ (e.g., $10^5$ pulses for $f_{PR} = 10$ MHz). The operating principle can be explained intuitively as follows. For simplicity, let us assume that the delay generator (DG) provides a delay equal to the entire time-of-flight (round trip) of the transmitted and received pulses. If the target is not moving (static target), the local replica and the amplified echo are aligned and the multiplier provides the same output pulse with pulse repetition frequency $f_{PR}$, as shown in Fig. 2(b), case (a). Therefore, the signal at the output of the integrator is pretty much constant, as shown in Fig. 2(c). Note that the integrator will provide a constant output voltage regardless of the relative shift ($\delta$) between the local replica and amplified echo, for any other constant $\delta$. If the target is moving, the movement causes a time-varying $\delta$ between the local replica and the eco amplified by the LNA. Therefore, the multiplier provides an output pulse that may be positive, negative o zero, depending on the $\delta$ caused by the time-varying distance between radar and target and due to the target movements around its quiescent position.

The radar sensor is thought to operate in two operating modes: ranging mode (RM) and tracking mode (TM). In RM
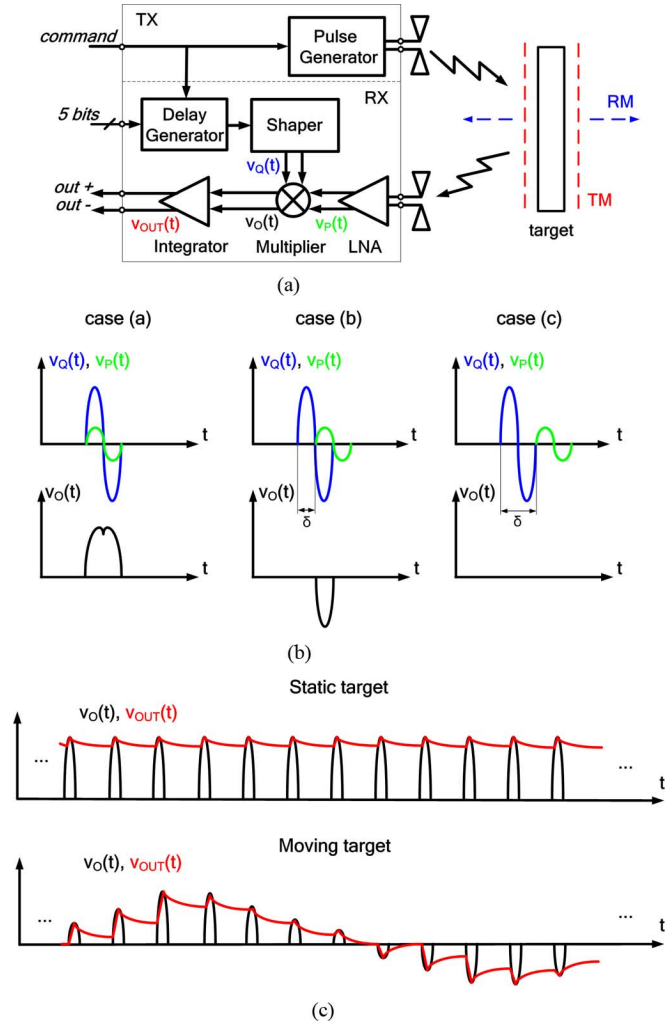
Fig. 2. (a) Block diagram of the SoC UWB pulse radar. The dashed lines around the target indicate the range spanned by the radar in RM and TM. (b) Representation of the pulses at the input and output of the multiplier for three different cases of relative shift ($\delta$) between the input pulses. (c) Representation of the input and output voltages of the integrator for static and moving targets.

the DG provides a variable delay in order to span the range of interest and identify the target [see Fig. 2(a)] [6]. In RM the radar sensor allows us to identify the presence of the target and the time of flight. When the target is detected, the radar can switch to the TM, in which the DG provides a fixed delay (i.e., equal to the time of flight identified in RM) in order to monitor a fixed range gate [see Fig. 2(a)] [6]. Therefore, the output voltage is directly sensitive to the target movements, e.g., the chest movement due to the pulmonary activity in case of respiratory rate monitoring. The output voltage can be expressed approximately as follows:

$$v_{OUT}(t) \approx A \frac{B}{2\pi} \int_{t-2\pi/B}^{t} v_Q(\tau) \times v_P(\tau) d\tau$$

$$\approx A \frac{B}{2\pi} \int_{t-2\pi/B}^{t} v_Q(\tau) \times \alpha \times v_Q(\tau - \delta) d\tau \quad (1)$$

which is obtained assuming that the amplified echo has the same shape of the transmitted pulse (i.e., the same of the local replica),

but different amplitude ($\alpha$ is the attenuation factor, A is the correlation gain, B is the bandwidth of the low-pass filter and $\delta$ the relative delay between the input signals of the multiplier).

### B. Design and Measurements

All the circuits have been designed according to the specifications derived by the feasibility study in [10]. They have fully differential topologies for better immunity to EMI and noise, and linearity.

The PG of Fig. 3(a) has been designed by following the principle in [9]. The idea consists of overdriving a shaping network (SN) by means of a triangular monocycle pulse generator. The SN is implemented by means of a CMOS source coupled differential pair. The triangular monocycle pulse is realized by means of the combination of two triangular pulses obtained by two identical triangular pulse generators (TPGs), of which the second one is activated after a delay equal to the duration time of the triangular pulse. The PG provides a monocycle pulse on the $100\,\Omega - \mathrm{diff}$ antenna when activated by the negative edge of the digital signal command with frequency $f_{PR}$. The PG, tested individually on the same die of the SoC radar, exhibits pulses with a duration time ($t_D$) of 350 ps and amplitude 650 mVpp-diff (including the losses of microprobes and cables) corresponding to about 900 mVpp-diff on-chip. The power consumption is 19.8 mW. The energy consumption ($E_C$) per transmitted pulse is $19.8\,\mathrm{mW} \times 350\,\mathrm{ps} = 6.9\,\mathrm{pJ}$. The PG exhibits the highest pulse amplitude, voltage (55%) and energy (3%) efficiencies, and robustness to PVT variations reported in the literature (references therein [9]). The output pulses are reported in Fig. 4(a) for $f_{PR} = 10\,\mathrm{MHz}$. The power spectral density (PSD) is reported in Fig. 4(b). Note the compliance with the UWB mask.

The Shaper of Fig. 2 adopts the same structure of the PG, but it requires a lower bias current (2mA) for its shaping network since it has a different load impedance (i.e., the input impedance of the multiplier). The power consumption is 13.8 mW.

The UWB LNA of Fig. 3(b) has been implemented according to the design in [11]. It consists of a common-gate stage, which realizes a wideband input impedance matching to the $100\,\Omega$-diff antenna, and two subsequent common-source stages which increase the overall gain. The power consumption in high-gain mode is 34.8 mW. Fig. 5 reports the main performance of the LNA tested as stand-alone. Note that $|S_{21}| = 22.7$ dB at 5 GHz, $|S_{11}| < -10.5$ dB and NF $= 6.5$ dB (including the noise contributions of UWB baluns, probes and cables) over the all UWB band. The input $P_{1\,\mathrm{dB}}$ is $-19.7$ dBm. This circuit solution exhibits one of the highest transducer gains (references therein [11]).

The UWB multiplier of Fig. 3(c) has been designed by following the principle in [12]. It exploits a p-MOSFET ($M_P$) common-gate pair input stage in order to provide a low-complexity input matching to the LNA output impedance ($\sim 200\,\Omega - \mathrm{diff}$) over a wide band. The multiplier stage consists of a p-MOSFET ($M_Q$) Gilbert quad. The common-mode feed-back (CMFB) regulates the common-mode output voltage through $V_{CM}$ and $V_C$. $V_{REF}(0.6\,\mathrm{V})$ is an external dc voltage reference. The power consumption is 3.7 mW. The multiplier has been tested as stand-alone by applying two sequences of pseudo-Gaussian monocycle pulses with
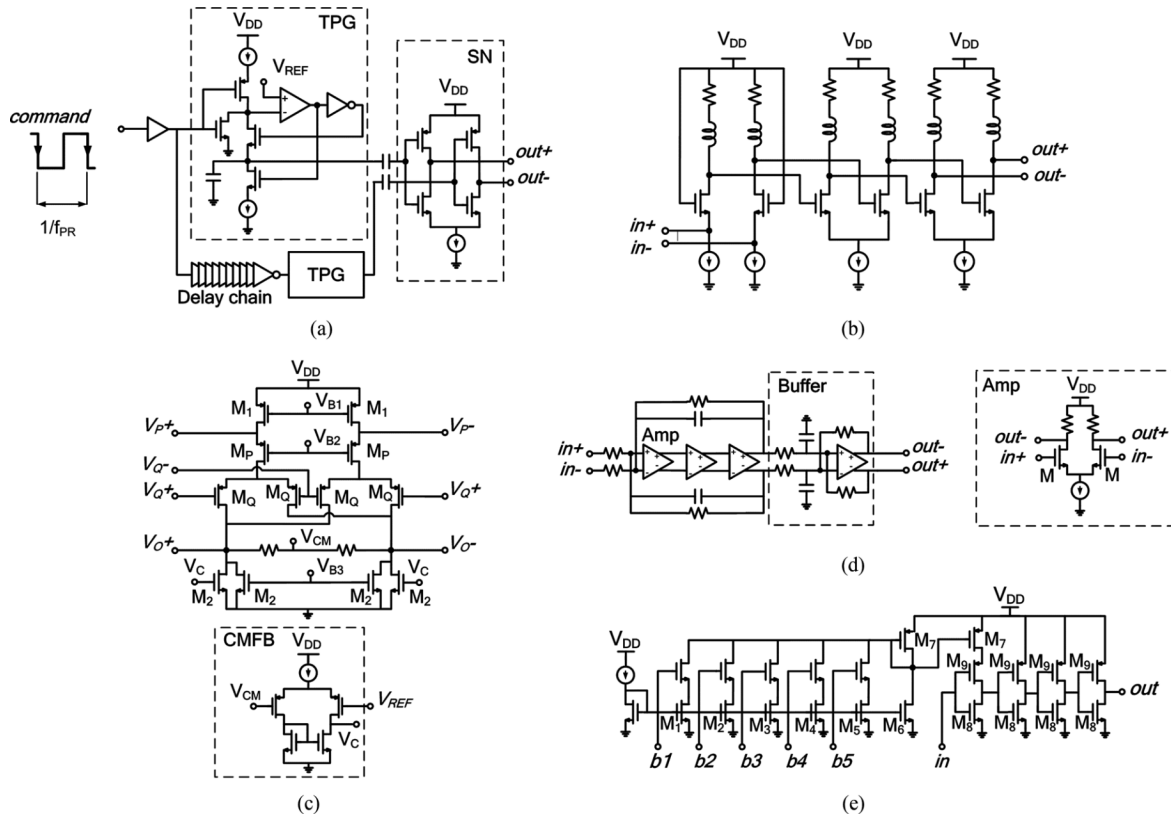
Fig. 3. Building blocks (schematics) of the SoC UWB pulse radar. (a) Pulse generator (TPG is for 'triangular pulse generator', SN is for 'shaping network'). (b) LNA. (c) Multiplier. (d) Integrator. (e) Delay generator. The power supply $(V_{DD})$ is 1.2 V.
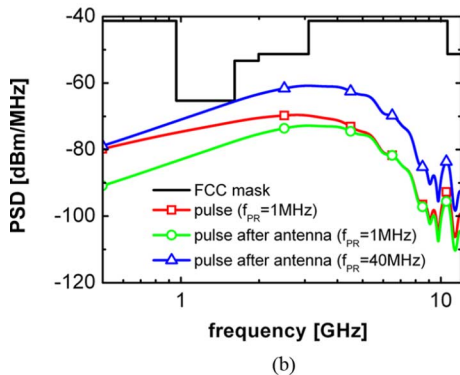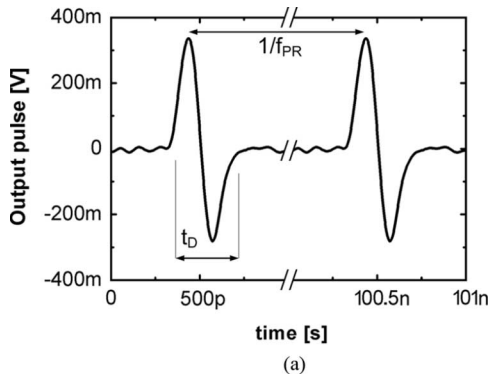


Fig. 4. (a) Output pulses provided by PG ($f_{PR} = 10$ MHz) captured by means of a two-channel ($50 \, \Omega-$ impedance each) real-time digital oscilloscope DSA 91204A (40 GSa/s, 12-GHz bandwidth). (b) Spectrum of the measured pulses before and after the antenna filtering and UWB mask by FCC.
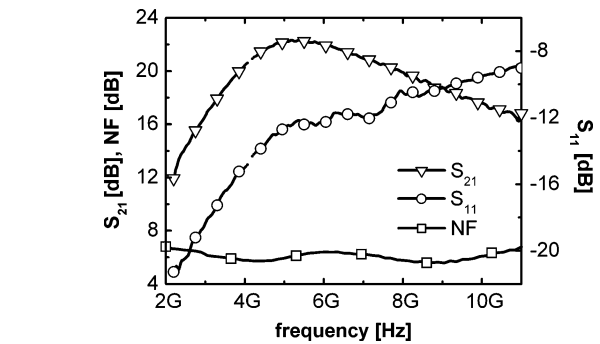


Fig. 5. LNA measurements (S parameters, $S_{21}$ and $S_{11}$, and noise figure, NF).

amplitude 170 mVpp-diff $(V_P)$ and 650 mVpp-diff $(V_Q)$, and $t_D = 700$ ps ($V_P$ is expected to be the echo amplified by the LNA, whereas $V_Q$ the delayed replica generated on-chip by the Shaper). Fig. 6 reports the output voltage $(V_O)$ for 3 different relative delays between the input pulses $V_P$ and $V_Q$. The NF is 14.4 dB at 4 GHz. The $P_{1 \, dB}$ is $-3.5$ dBm and $-2$ dBm for P and Q inputs, respectively. This circuit solution allows us to implement efficiently the multiplication between short pulses, with improved performance with respect to the state of the art (SoA) in terms of $P_C$, NF and $P_{1 \, dB}$ (references therein [12]).

The integrator of Fig. 3(d) consists of a 3-stage amplifier with RC feedback and output buffer. The stages use identical differential pair amplifiers. Details of the devices sizing are reported in [6]. The power consumption is 1.1 mW. The voltage gain is 58 dB and $B_{3 \, dB} = 147$ Hz.
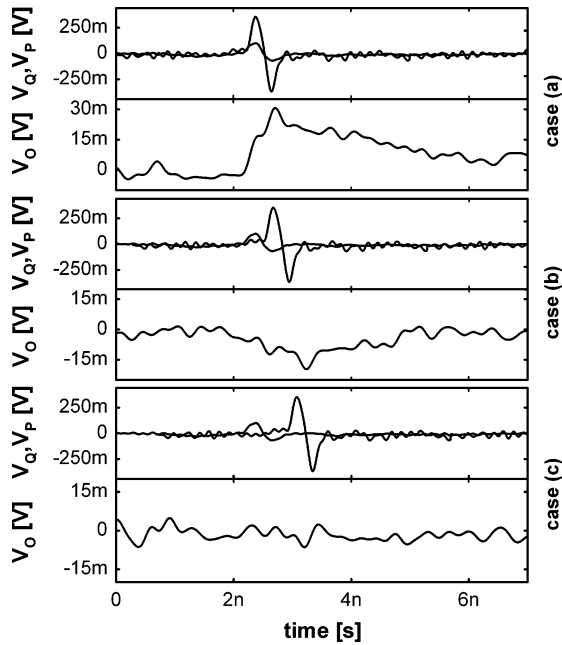
Fig. 6. I/O signals of the multiplier measured in three cases: the input mono-cycle pulses have (a) no relative delay (i.e., time alignment), (b) a relative delay of half of the time duration, and (c) relative delay equal to the time duration. $V_O$ is captured by the probe 1134A (impedance $50\,\mathrm{K}\Omega \| 0.27\,\mathrm{pF}$) and oscilloscope DSO 54855A.
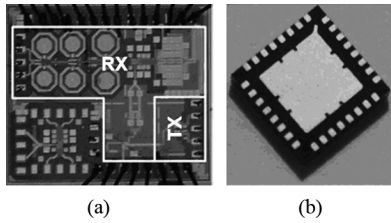


Fig. 7. SoC UWB pulse radar. (a) Micrograph of the radar testchip (all pads are ESD protected). The die size is $1.5 \times 1.3\,\mathrm{mm}^2$ (including the multiplier as stand-alone device). (b) Radar testchip packaged in a QFN32 leadless package (bottom view) with exposed ground pad (size $5 \times 5\,\mathrm{mm}^2$).

The 5-bit programmable monotonic delay generator (DG) of Fig. 3(e) has been designed following the principle in [13]. Details of the devices sizing are reported in [6]. The 5 bits allow us to select the output current of the inverter ($M_8$ and $M_9$) in order to vary the slope of the voltage ramp (high to low) across its load capacitance. By varying the bias current, the DG can provide delays in the range 1 to 30 ns. The power consumption is lower than 0.1 mW.

Fig. 7 shows the radar testchip both onto die and package. The die size ($2\,\mathrm{mm}^2$) reflects the impact on area of the SoC approach (e.g., $4\,\mathrm{cm}^2$ for discrete radars for similar applications [7]). The overall $P_C$ is 73.2 mW (bias inclusive), which is lower than CW radars for similar applications (reference therein [6]). The radar packaged in QFN32 was mounted on a test-board including the antennas (TX and RX) with 2.3 dBi gain at 3.5 GHz, $|S_{11}| < -10\,\mathrm{dB}$ in the band 2.8 to 5.4 GHz covering the range of interest from 3 to 5 GHz. The test-board ($10 \times 13\,\mathrm{cm}^2$) has been implemented on FR4 substrate ($h = 1.6\,\mathrm{mm}, t = 35\,\mu\mathrm{m}$). The complete test setup is shown in Fig. 8. The radar detected
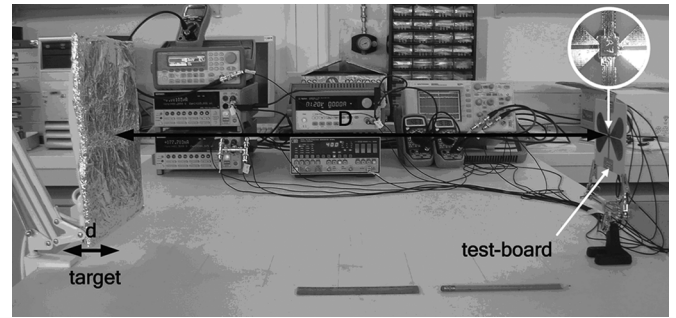


Fig. 8. Experimental setup for the characterization of the UWB pulse radar sensor, including packaged SoC pulse radar and on-board antennas. The target is made of a 0.5 cm-thick board covered by an aluminum foil. The radar sensor is placed at a distance (D) from the target which may move for a displacement (d). A detail of the packaged radar testchip mounting on test-board is reported in the insert on top right corner.
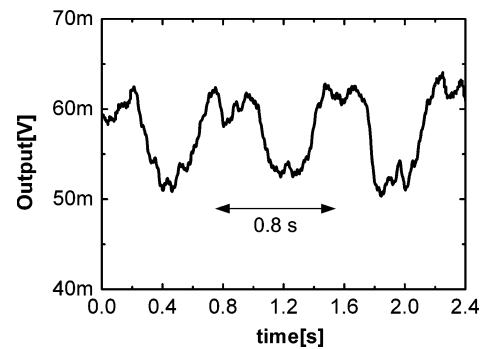


Fig. 9. Output voltages (measured) in TM ($f_{PR} = 40\,\mathrm{MHz}$). The target movement rate is 1.25 Hz.

3 targets with different areas ($26 \times 26$, $13 \times 26$ and $13 \times 13\,\mathrm{cm}^2$) for movements (front-back) up to a displacement (d) of 2cm around a distance (D) up to 70 cm. Fig. 9 reports the output voltage for the target of area $26 \times 26\,\mathrm{cm}^2 (\mathrm{d} = 2\,\mathrm{cm}, \mathrm{D} = 70\,\mathrm{cm})$. The power consumption of the receiver is 59.4 mW. $E_C$ per received pulse is $59.4\,\mathrm{mW} \times 0.6\,\mathrm{ns} = 36\,\mathrm{pJ}$ ($t_D$ of the echo captured by the antenna is about 0.6 ns). The experimental results demonstrate that the radar sensor detects the target movements despite the output voltage indicates a limited signal-to-noise ratio. This is due fundamentally to the very low level of received power, which is mainly related to the low level of transmitted power, target reflectivity, radar cross-section, distance and interferences. Note that the dc offset ($\sim 55\,\mathrm{mV}$), which can be eliminated by means of digital processing, is not an issue for this application aimed at detecting the movement rate.

## III. RESPIRATORY RATE MONITORING: EXPERIMENTAL TESTS

Fig. 10 shows three different application scenarios (S1, S2 and S3) of the radar sensor (microchip packaged mounted on the microstrip test-board with antennas).

In S1 [see Fig. 10(a)], a 39-years old person (male) under test is awake and seated in front of the radar sensor at $D = 25\,\mathrm{cm}$. The body mass index (BMI) [14] of the person under test is 26.9 Kg/m$^2$. The maximum chest displacement (d) during respiration was about 1 cm.
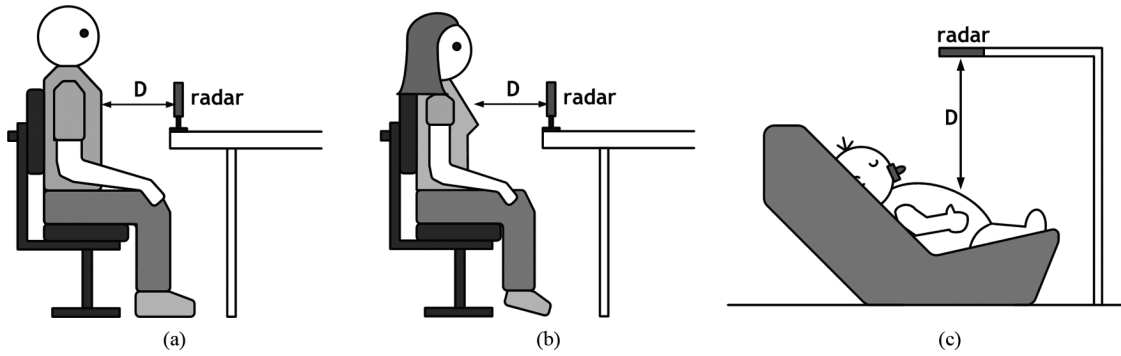
Fig. 10.   The three experimental scenarios (S1, S2 and S3) for the field operational tests of the radar sensor. (a) S1: a 39-years old male (188 cm height, 95 kg weight, awake) is seated in front of the UWB radar sensor. (b) S2: a 30-years old female (170 cm height, 60 kg weight, awake) is seated in front of the UWB radar sensor. (c) S3: a 5-month old baby girl (65 cm height, 8 kg weight, asleep) is in a baby car seat placed under the radar sensor at a distance $D = 30$ cm from the her chest.
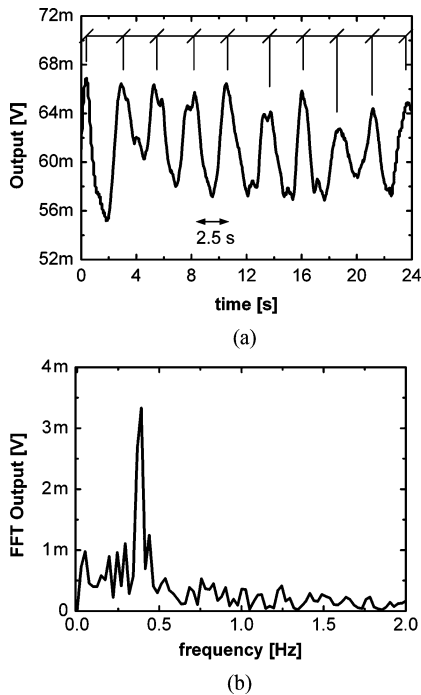


Fig. 11.   Output voltage (measured) in TM ($f_{PR} = 40$ MHz) for S1. The respiratory rate is about 0.4 Hz a) time domain b) frequency domain (i.e., FFT of the time-domain waveform after dc offset cancellation).
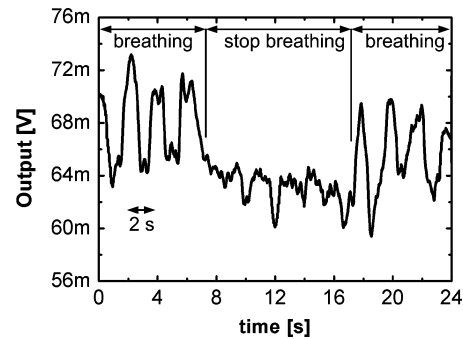


Fig. 12.   Output voltage (measured) in TM ($f_{PR} = 40$ MHz) for S1. In the first phase of the experiment the person under test is breathing; in the second phase the person under test is holding voluntarily his breath; in the third phase the normal respiration process is restored.
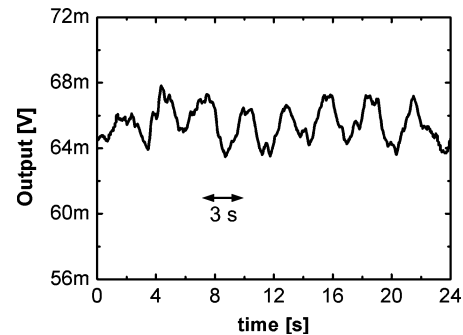


Fig. 13.   Output voltage (measured) in TM ($f_{PR} = 40$ MHz) for S1 for a distance $D = 45$ cm. The respiratory rate is about 0.33 Hz.

The measurements reported in Fig. 11 show that the radar detects the respiratory rate ($\sim 0.4$ Hz).

Fig. 12 shows the output voltage during an additional experiment carried out in S1, in which the person under test is initially breathing and after stops voluntarily breathing. Note how the radar sensor tracks the entire profile of the respiration. This is an important aspect especially considering the limitations of existing contact technologies using electrodes, wires or piezoelectric materials, which are very prone to motion artifacts [15], e.g., caused by variation of the contact resistance of the electrodes. Similar performance have been measured up to $D = 45$ cm as reported in Fig. 13.

In S2 [see Fig. 10(b)], a 30-years old person (female, whose chest differs from male, with BMI of $20.8$ Kg/m$^2$) under test is awake and seated in front of the radar sensor at $D = 30$ cm.

The measurements reported in Fig. 14 show that the radar detects the respiratory rate ($\sim 0.3$ Hz). The maximum chest displacement (d) during respiration was about 0.7 cm. Similar performance have been measured up to $D = 40$ cm. In S3 [see Fig. 10(c)], a five-month baby (female with BMI of $18.9$ Kg/m$^2$) is seated in a car seat placed under the radar sensor. The baby is sleeping and her chest is at $D = 30$ cm from the radar sensor. The measurements in Fig. 15 show that the radar detects the respiratory rate in two different observation intervals of the baby under test [$\sim 0.4$ Hz in Fig. 15(a) and $\sim 0.5$ Hz in Fig. 14(b)]. The maximum chest displacement during respiration was about 2 mm. Similar performance have
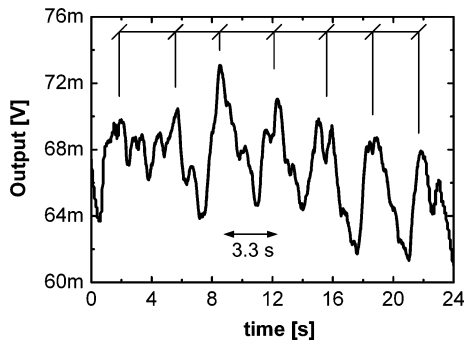
Fig. 14. Output voltage (measured) in TM ($f_{PR} = 40$ MHz) for S2. The respiratory rate is about 0.3 Hz.



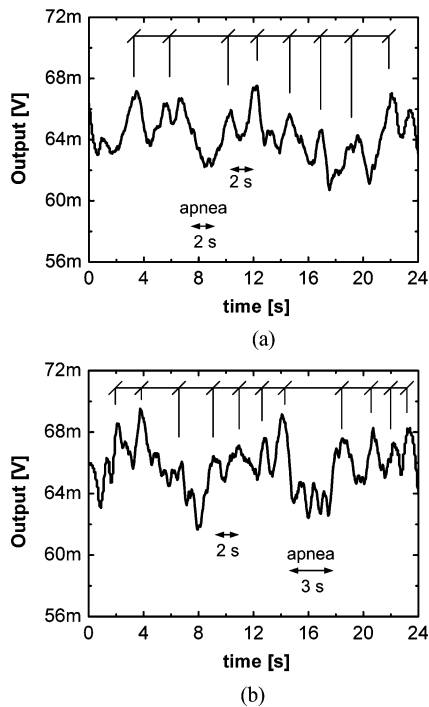Fig. 15. Output voltages (measured) in TM ($f_{PR} = 40$ MHz) for S3 for two different sleep time intervals. The respiratory rate is slightly irregular with an average of 0.4 Hz in (a) and 0.5 Hz in (b). Note that the radar detects very short apneas of 2s (a) and 3s (b).

been measured up to $D = 35$ cm. Note that measurements in Figs. 15(a)–15(b) show that the radar tracks the respiratory activity of the baby under test during sleep with a slightly irregular breathing. Moreover, note that the radar sensor output voltage is capable of detecting very short sleep apneas [$\sim 2$ s in Fig. 15(a) and $\sim 3$ s in Fig. 15(b)] in which the baby stops breathing during sleep and the output voltage remains constant except for small amplitude variations approximately lower than 2 mV due to noise. It is worth saying that irregular breathing with fast and slow phases and very short apnea events happen very frequently in babies under six months and therefore they do not represent a pathology, at least in this case under test (typically abnormal apneas are longer than 10–20s). All these results are intended to demonstrate that the UWB pulse radar sensor proposed is capable of detecting the respiratory rate of adults (regardless of the gender) and babies in some of the possible operating scenarios investigated by means of the field experimental tests described above.

## IV. CONCLUSIONS

A system-on-chip UWB pulse radar based on correlation receiver has been implemented in 90 nm bulk CMOS technology, characterized experimentally and applied to respiratory rate monitoring. The experimental tests on adult (both genders) and baby have been carried out successfully in different scenarios, demonstrating that the UWB pulse radar sensor is capable of detecting the respiration activity associated with sub-centimeter chest movements.

This UWB contactless sensing technology could be potentially employed in a variety of mass-market applications, as for constant monitoring of babies in cot beds, hospital patients and other people at risk of obstructive apneas including, sudden infant death syndrome (SIDS). It can be used also for the early detection of sudden sleep of drivers in vehicles. This UWB sensing technology also enables several other important applications such as facilitating patients in being monitored in their home, with data sent in real-time through the network to general practitioners (GPs) and first-aid medical staff in hospitals. It can also be used for fitness (fatigue) monitoring and personalized healthcare for independent and healthy living. In spite of its applications to the biomedical field, the SoC UWB pulse radar sensor can be also applied to other civil applications requiring contactless detection of moving objects non transparent to UWB radiation. Future works are addressed to the design of advanced prototypes including digital circuits for its validations in large-scale clinical trials and commercialization.

## REFERENCES

[1] European Commission, FP7 Health—Orientation Paper [Online]. Available: http://cordis.europa.eu/fp7/health
[2] H.-S. P. Wong, D. J. Frank, P. M. Solomon, C. H. J. Wann, and J. J. Welser, "Nanoscale CMOS," *Proc. IEEE*, vol. 87, no. 4, pp. 537–570, Apr. 1999.
[3] Revision of Part 15 of the Commission's Rules Regarding Ultra-Wideband Transmission Systems, FCC 02–48 2002.
[4] W. Karlen, C. Mattiussi, and D. Floreano, "Sleep and wake classification with ECG and respiratory effort signals," *IEEE Trans. Biomed. Circuits Syst.*, vol. 3, no. 2, pp. 71–78, Apr. 2009.
[5] S. M. Caples, A. S. Gami, and V. K. Somers, "Obstructive sleep apnea," *Ann. Internal Med.*, vol. 142, no. 3, pp. 187–197, Feb. 2005.
[6] D. Zito, D. Pepe, M. Mincica, and F. Zito, "A 90 nm CMOS SoC UWB pulse radar for respiratory rate monitoring," in *Proc. IEEE Int. Solid-State Circuits Conf. Dig. Tech. Paper*, Feb. 2011, pp. 41–42.
[7] S. G. Azevedo and T. E. McEwan, "Micropower impulse radar," *Sci. Technol. Rev.*, pp. 17–29, Jan./Feb. 1996.
[8] I. Immoreev and T.-H. Tao, "UWB radar for patient monitoring," *IEEE Aerosp. Electron. Syst. Mag.*, vol. 23, no. 11, pp. 11–18, Nov. 2008.
[9] F. Zito, D. Pepe, and D. Zito, "UWB CMOS monocycle pulse generator," *IEEE Trans. Circuits Syst I, Reg. Papers*, vol. 57, pp. 2654–2664, Oct. 2010.
[10] D. Zito *et al.*, "Wearable system-on-a-Chip UWB radar for health care and its application to the safety improvement of emergency operators," in *Proc. IEEE Dig. Int. Conf. Engineering in Medicine and Biology Society*, Aug. 2007, pp. 2651–2654.

[11] D. Pepe and D. Zito, "22.7 dB gain -19.7 dBm iCP1 dB UWB CMOS LNA," *IEEE Trans. Circuits Syst. II, Exp. Briefs*, vol. 56, no. 9, pp. 689–693, Sep. 2009.

[12] M. Mincica, D. Pepe, and D. Zito, "CMOS UWB multiplier," *IEEE Trans. Circuits Syst. II, Exp. Briefs*, vol. 58, no. 9, pp. 570–574, Sep. 2011.

[13] M. Maymandi-Nejad and M. Sachdev, "A monotonic digitally controlled delay element," *IEEE J. Solid-State Circuits*, vol. 40, pp. 2212–2219, Nov. 2005.

[14] A. H. Mokdad *et al.*, "Prevalence of obesity, diabetes and obesity-related health risks factors," *J. Amer. Med. Assoc.*, vol. 289, no. 1, pp. 76–79, Jan. 2003.

[15] A. Lanatà, E. P. Scilingo, E. Nardini, G. Loriga, R. Paradiso, and D. De-Rossi, "Comparative evaluation of susceptibility to motion artifact in different wearable systems for monitoring respiratory rate," *IEEE Trans. Inf. Technol. Biomed.*, vol. 14, no. 2, pp. 378–386, Mar. 2010.

**Domenico Zito** (S'00–M'04) received the M.Sc. degree in electronic engineering and the Ph.D. degree in information engineering from the University of Pisa, Pisa, Italy, in 2000 and 2004, respectively.

He was a Visiting Researcher at STMicroelectronics, Catania, Italy, in 2001, and Austriamicrosystems, Graz, Austria, in 2002. In 2005, he was appointed as an Assistant Professor of electronics at the University of Pisa. Since March 2009, he has been with University College Cork and Tyndall National Institute, Cork, Ireland, as a "G. G. Stokes" Lecturer in microelectronic engineering. His primary scientific interests are the design of system-on-chip radiofrequency (microwave and millimeter-wave) front-ends in standard CMOS and Bi-CMOS technologies for emerging wireless applications (data communication and contactless sensing). He is the author of more than 80 papers in peer-reviewed international journals and conference proceedings (six invited papers), two chapters of book, two books (one book edited) and two patents. He is WP Leader and Principal Investigator of national and international research projects.

Dr. Zito is on the Reviewers' Board of several peer-reviewed international journals and is serving as a Member and Chair of the Technical Program Committee in IEEE international conferences. He was the recipient of the First Price at European Wireless Business Idea Competition "Mario Boella" in 2005. He received three awards and two best paper award nominations in IEEE conferences.

**Domenico Pepe** (S'08-M'09) received the B.Sc. and the M.Sc. degrees in electronic engineering from the University of Pisa, Pisa, Italy, in 2002 and 2005, respectively, and the Ph.D. degree from the University of Pisa, in joint supervision with the University of Bordeaux 1, Bordeaux, France, in 2009.

In 2007, he was a visiting Ph.D. student at the IMS Laboratory, Bordeaux, France, working on the design of 60 GHz LNA in 65 nm CMOS technology. He is currently a Postdoc Research Fellow at Tyndall National Institute, Cork, Ireland. His research interests are in the areas of radio-frequency and millimeter-wave ICs design for communication and sensing applications.

**Martina Mincica** (S'10) received the B.Sc., M.Sc., and Ph.D. degrees in electronic engineering from University of Pisa, Pisa, Italy, in 2004, 2007, and 2011, respectively.

Her primary research interest is the radiofrequency integrated circuits design. She is now with Analog Devices, Limerick, Ireland.

**Fabio Zito** received the B.Sc., M.Sc., and Ph.D. degrees in electronic engineering from University "Mediterranea" of Reggio Calabria, Reggio Calabria, Italy, in 2003, 2006, and 2010, respectively.

He was a visiting M.Sc. and a Ph.D. student at the University of Pisa, Pisa, Italy, working on radiofrequency ICs design in 90 nm CMOS technology. His research interests are the design of VLSI systems for radio-frequency identification devices. He is now with Ansaldo STS SpA, Naples, Italy.

**Alessandro Tognetti** received the M.Sc. degree in electronic engineering and the Ph.D. degree in robotics, automation, and bioengineering from the University of Pisa, Pisa, Italy, in 2001 and 2005, respectively.

He is currently a Postdoctoral Researcher at the Interdepartmental Research Center "E. Piaggio," University of Pisa, where he is engaged in the design and development of wearable kinesthetic interfaces for human posture and movement detection. He is the author or coauthor of several papers and has contributed to international conferences and chapters in international books. His current research interests include sensor design and signal and information processing.

**Antonio Lanatà** received the M.Sc. degree in electronic engineering and the Ph.D. degree in automation, robotics and bioengineering from the University of Pisa, Pisa, Italy, in 2001 and 2006, respectively.

He is a Postdoctoral Research Fellow at the Interdepartmental Research Centre "E. Piaggio", University of Pisa. His research interests include wireless wearable systems for health status monitoring by ultrasound-acoustic technology and signal processing.

**Danilo De Rossi** (M'91) received the Laurea degree in chemical engineering from the University of Genoa, Genoa, Italy, in 1976.

From 1976 to 1981, he was a Researcher at the Institute of Clinical Physiology, National Research Centre, Pisa, Italy. He had appointments for teaching and research in Australia, Brasil, France, Japan, and USA. In 1982, he joined the Faculty of Engineering, University of Pisa, Pisa, Italy, where he is currently a Full Professor of bioengineering in the Interdepartmental Research Center "E. Piaggio". His scientific activities are related to the physics of organic and polymeric materials, and to the design of sensors and actuators for bioengineering and robotics. He is the author or coauthor of more than 270 peer reviewed papers published in various international science journals and peer reviewed proceedings. He is the coinventor of 14 patents and coauthor of eight books.

Prof. De Rossi was the recipient of the Bioengineering Forum Award of the Biological Engineering Society (U.K.) in 1980 and the Young Investigator Award of the American Society for Artificial Organs (USA) in 1985.